A CONVEX VARIATIONAL MODEL FOR RESTORING BLURRED IMAGES WITH RICIAN NOISE

LIYUAN CHEN* AND TIEYONG ZENG †

Abstract. In this paper, a new convex variational model for restoring images degraded by blur and Rician noise is proposed. The new method is inspired by previous works in which the non-convex variational model obtained by MAP estimation has been presented. Based on the statistical property of Rician noise, we put forward to adding a quadratic penalty term into it, which leads a new strictly convex model under mild condition. The new model guarantees the uniqueness of the solution and stabilization of the algorithm. We utilize a primal-dual algorithm to solve the model. Numerical results are presented in the end to demonstrate that our model outperforms some of the state-of-the-art models in both medical and natural images.

Key words. Convexity, deblurring, primal-dual method, Rician noise, total variation.

AMS subject classifications. 52A41, 65K10, 65K15, 90C30, 90C47

1. Introduction.

In digital image processing, most real images are generated through image recording systems. During the formation procedure, images are unavoidably corrupted by noise and blurring. Hence, in the domain of image processing, the image restoration under various noises and blurring is always one of the fundamental tasks. As the additive Gaussian white noise is the most typical noise in image formation, many approaches have been proposed to remove Gaussian noise [10, 12, 13, 19, 24, 36]. In the literature, depending on the imaging systems, various other kinds of noises have also been considered, such as Impulse noise [11, 17, 22], Poisson noise [30, 41] and multiplicative noise [4, 23]. In recent years, with the development of Magnetic Resonance Imaging (MRI), another very important noise, Rician noise, has been taken into account gradually. Indeed, Rician noise frequently occurs in the magnitude image where the real and imaginary components of the image are both corrupted by Gaussian noise. It has been verified that Rician noise can be approximated rather well by homogenous Gaussian noise in the case of high SNR, but in the low SNR case, the Rician noise can not be so readily approximated [2, 7]. Hence, it is important to develop techniques for image recovery under Rician noise.

Mathematically, suppose that an image u is a real function defined on Ω, a connected bounded open subset of $\mathbb{R}^2$ with compact Lipschitz boundry, i.e., $u : \Omega \to \mathbb{R}$. The format of the measured degraded image f under Rician noise is given by,

$$f = \sqrt{(Au + \eta_1)^2 + \eta_2^2}, \tag{1.1}$$

where $A \in \mathcal{L}(L^2(\Omega))$ is a known linear blurring operator, and η_1, η_2 represent independent Gaussian white noise of standard deviation σ. Here, the observed image f is firstly blurred by the blurring operator A, and then is corrupted by the Rician noise. Usually we assume that $f > 0$. In this paper, we pay attention to the assumption that the blur is the identity operator (for denoising), Gaussian blur or Motion blur.

In the literature, various methods have been proposed to deblur and denoise the magnitude image corrupted by blur and Rician noise. In [25,34], Anisotropic Diffusion

*Department of Mathematics, Hong Kong Baptist University, Kowloon Tong, Hong Kong. (12466212@life.hkbu.edu.hk)

†Department of Mathematics, Hong Kong Baptist University, Kowloon Tong, Hong Kong. (zeng@hkbu.edu.hk)

Filter (ADF) was proposed to solve the denoising problem with edge preservation. However, this method usually wipes small features. In [32], Nowak studied wavelet-domain filtering methods for Rician noise removal. In [39], Wood and Johnson came up with using wavelet packet denoising method to remove Rician noise. Although the wavelet approaches are effective to preserve image details and features without compromising edge sharpness, they are apt to introduce characteristic artifacts (small pots) which can hamper the image analysis process [31]. In [8], Basu *et al.* proposed a new method for denoising diffusion tensor images that includes a Rician noise model as part of MAP estimation framework. This was the first work to explicitly model and remove the bias effects of Rician noise in Diffusion Tensor MRI image. In [38], inspired by [21, 37], Daesslé*et al.* developed a non-local means (NLMeans) filter for Rician noise removal. In [26], based on the maximum a posteriori (MAP) estimation, Getreuer *et al.* proposed a total variational (TV) model as follows,

$$\inf_u \frac{1}{2\sigma^2}\int_\Omega u^2 dx - \int_\Omega \log I_0(\frac{fu}{\sigma^2})dx + \gamma \mathrm{TV}(u), \tag{1.2}$$

where I_0 is the zero order Modified Bessel function [1] and $\mathrm{TV}(u)$ is the classical total variation prior. Unfortunately, (1.2) is non-convex due to the second term. In order to overcome this issue, they further considered the following convex model to approximate (1.2),

$$\inf_u \gamma \mathrm{TV}(u) + \int_\Omega G_\sigma(u,f)dx, \tag{1.3}$$

where letting $c = 0.8246$, we have,

$$\begin{aligned} G_\sigma(u,f) &= \begin{cases} H_\sigma(u) & \text{if} \quad u \geq c\sigma, \\ H_\sigma(c\sigma) + H'_\sigma(c\sigma)(u - c\sigma) & \text{if} \quad u \leq c\sigma, \end{cases} \\ H'_\sigma(u) &= \frac{u}{\sigma^2} - \frac{f}{\sigma^2} B(\frac{fu}{\sigma^2}), \\ B(t) &\equiv \frac{I_1(t)}{I_0(t)} \approx \frac{t^3 + 0.950037t^2 + 2.38944t}{t^3 + 1.48937t^2 + 2.57541t + 4.65314}. \end{aligned}$$

Here, $H_\sigma(u)$ is the primitive function of $H'_\sigma(u)$. In the rest of the paper, we call it Getreuer's model for short.

Evidently, the model (1.3) is somewhat complex and its mathematical property is difficult to derive. The goal of this paper is to provide a new elegant convex model for Rician noise removal. Since TV regularization is extremely effective for recovering "blocky", possibly discontinuous, functions from noisy data with reserving sharp edges of images [12, 16], in our paper, we still use this regularization and it could be readily replaced by some other modern regularization terms such as non-local TV or framelet approach. However, different from Getreuer's model, we add a reasonable quadratic penalty term into the non-convex model (1.2) to derive a new convex model. By this, we can guarantee the uniqueness of the solution. The minimization of our model can be efficiently handled by the primal-dual algorithm [6, 14, 20, 22, 40, 42]. The numerical results in this paper show that our method has the potential to outperform the other approaches in Rician noise removal with deblurring simultaneously.

The rest of the paper is organized as follows. In Section 2, we briefly review the total variation regularization and introduce its main properties. In Section 3, based on the statistical properties of the Rician noise, we propose a new convex model for denoising, and discuss the condition to ensure its convexity. Meanwhile, the existence and the uniqueness of the solution are also proved in this section. In Section 4, we extend the model to the case of denoising and deblurring simultaneously and present the corresponding properties. Section 5 gives the primal-dual algorithm for solving our convex restoration models. The numerical results shown in Section 6 demonstrate the superior performance of our approach. In the end, conclusion remarks are drawn in Section 7.

2. Review of Total Variation Regularization. In order to reserve sharp edges in images efficiently, in [36], Rudin et al. introduced the celebrated total variation (TV) regularization. In their approach, they considered image in $BV(\Omega)$, which means the space of functions of bounded variation, i.e. $u \in BV(\Omega)$ iff $u \in L^1(\Omega)$ and the BV-seminorm

$$\int_\Omega |Du| := \sup\left\{ \int_\Omega u \cdot \mathrm{div}(\xi(x))\mathrm{d}x \Big| \xi \in C_0^\infty(\Omega, \mathbb{R}^2), \|\xi\|_{L^\infty(\Omega,\mathbb{R}^2)} \leq 1 \right\}, \tag{2.1}$$

is finite. The space $BV(\Omega)$ with the norm $\|u\|_{BV} = \|u\|_{L^1} + \int_\Omega |Du|$ is a Banach space. If $u \in BV(\Omega)$, the distributional derivative Du is a bounded Radon measure and the above quantity defined in (2.1) corresponds to the total variation (TV). Based on the compactness of $BV(\Omega)$, in two-dimensional case we have the embedding $BV(\Omega) \hookrightarrow L^p(\Omega)$ for $1 \leq p \leq 2$ which is compact for $p < 2$. See [3, 5, 19] for more details.

3. A Convex Rician Denoising Model. Before we establish a convex Rician denoising model, let us recall some basic information of Rician noise which will be used in the sequel.

The noise in magnitude image is assumed to be Rician distribution because the noises added into the real and imaginary parts of the image both obey the same Gaussian distribution. In this paper, we suppose that the Gaussian distribution is $\mathcal{N}(0, \sigma^2)$. The description of the magnitude image corrupted by Rician noise can be written as follows,

$$\begin{aligned} f &= \sqrt{(u+\eta_1)^2 + {\eta_2}^2}, \\ \eta_1 \sim \mathcal{N}(0,\sigma^2), &\quad \eta_2 \sim \mathcal{N}(0,\sigma^2). \end{aligned} \tag{3.1}$$

Before we present the property of the magnitude image f, as a prerequisite, we firstly introduce a Lemma as follows.

LEMMA 3.1. *Assume that $a, b \in \mathbb{R}$. Then, $|(u^2+2au+b^2)^{\frac{1}{4}} - u^{\frac{1}{2}}| \leq \sqrt{|a|} + \sqrt{|b|}$ is true whenever $u \geq 0$ and $|a| \leq |b|$.*

Proof. Readily, we have the following inequalities,

$$\begin{aligned} (\sqrt{u} + \sqrt{|a|} + \sqrt{|b|})^2 &\geq u + |a| + |b|, \\ (\sqrt{u} - \sqrt{|a|} - \sqrt{|b|})^2 &\leq u - |a| \qquad \text{if} \quad \sqrt{u} \geq \sqrt{|a|} + \sqrt{|b|}, \\ (u^2 + 2au + b^2)^{\frac{1}{2}} &\geq u - |a| \qquad \text{if} \quad |b| \geq |a|. \end{aligned}$$

Using these inequalities, we can easily verify that,

$$\sqrt{u} - \sqrt{|a|} - \sqrt{|b|} \leq (u^2 + 2au + b^2)^{\frac{1}{4}} \leq \sqrt{u} + \sqrt{|a|} + \sqrt{|b|}.$$

Thus, the proof of Lemma 3.2 is finished. □

PROPOSITION 3.2. *Suppose that the variables* η_1 *and* η_2 *independently follow the Normal distribution* $\mathcal{N}(0,\sigma^2)$. *Set* $f=\sqrt{(u+\eta_1)^2+\eta_2^2}$ *where* u *is fixed and* $u\geq 0$. *Then we can get the following inequality,*

$$\frac{\mathbb{E}((\sqrt{f}-\sqrt{u})^2)}{\sigma}\leq\sqrt{\frac{2}{\pi}}(\pi+2). \tag{3.2}$$

Proof. Since (3.1), we can get,

$$\sqrt{f}-\sqrt{u}=(u^2+2\eta_1 u+\eta_1^2+\eta_2^2)^{\frac{1}{4}}-u^{\frac{1}{2}}.$$

Based on Lemma 3.1, we obtain

$$(\sqrt{f}-\sqrt{u})^2\leq\left(\sqrt{|\eta_1|}+\sqrt{(\eta_1^2+\eta_2^2)^{\frac{1}{2}}}\right)^2\leq 2\left(|\eta_1|+(\eta_1^2+\eta_2^2)^{\frac{1}{2}}\right).$$

Hence,

$$\mathbb{E}((\sqrt{f}-\sqrt{u})^2)\leq 2\mathbb{E}(|\eta_1|)+2\mathbb{E}((\eta_1^2+\eta_2^2)^{\frac{1}{2}}).$$

As we have already known, η_1 and η_2 follow Gaussian distribution $N(0,\sigma^2)$, on the basic of statistical theories, we have

$$Y:=\frac{\eta_1^2+\eta_2^2}{\sigma^2}\sim\chi^2(2),$$

which means that Y follows Chi-squared distribution with 2 degrees. Therefore, according to the PDF of normal variable and Chi-square variable with two degrees, we can calculate

$$\mathbb{E}(\sqrt{Y})=\frac{\mathbb{E}((\eta_1^2+\eta_2^2)^{\frac{1}{2}})}{\sigma}=\frac{\sqrt{2\pi}}{2},$$
$$\mathbb{E}(|\eta_1|)=\sqrt{\frac{2}{\pi}}\sigma.$$

Taken together,

$$\mathbb{E}((\sqrt{f}-\sqrt{u})^2)\leq(\sqrt{2\pi}+\frac{2\sqrt{2}}{\sqrt{\pi}})\sigma.$$

Thus we finish the proof of the Proposition. □

The Proposition 3.2 ensures that the value of $\frac{\mathbb{E}((\sqrt{f}-\sqrt{u})^2)}{\sigma}$ is always bounded. Numerically, we can verify that for natural images and typical medical images, the real value of $\frac{\mathbb{E}((\sqrt{f}-\sqrt{u})^2)}{\sigma}$ is usually very small. Indeed, in Table 3.1, we report the values of $\frac{\mathbb{E}((\sqrt{f}-\sqrt{u})^2)}{\sigma}$ for different values of σ with different original image u. Clearly, these values are very small.

In the denoising case, that is, A is the identity operator, from the degradation model (1.1), we obtain that $f=\sqrt{(u+\eta_1)^2+\eta_2^2}$. Inspired by Proposition 3.2, we now introduce a quadratic penalty term into the MAP model (1.2), which turns out to be

$$\inf_{u\in\bar{S}(\Omega)}\frac{1}{2\sigma^2}\int_\Omega u^2dx-\int_\Omega\log I_0(\frac{fu}{\sigma^2})dx+\frac{M}{\sigma}\int_\Omega(\sqrt{u}-\sqrt{f})^2dx+\gamma\mathrm{TV}(u), \tag{3.3}$$

Image	$\sigma=5$	$\sigma=10$	$\sigma=15$	$\sigma=20$	$\sigma=25$	$\sigma=30$
Cameraman	0.0261	0.0418	0.0571	0.0738	0.0882	0.1040
Bird	0.0131	0.0255	0.0371	0.0486	0.0590	0.0685
Skull	0.0453	0.0754	0.1009	0.1234	0.1425	0.1600
Leg joint	0.0356	0.0654	0.0906	0.1105	0.1263	0.1419

TABLE 3.1

The values of $\frac{\mathbb{E}((\sqrt{f}-\sqrt{u})^2)}{\sigma}$ *for different values of* σ *with different original image* u.

with the penalty parameter $M > 0$. In addition, we set

$$\bar{S}(\Omega) := \{v \in BV(\Omega) : v \geq 0\},$$

which is closed and convex. In the coming section, we will show that if M is big enough, the above model is strictly convex.

In medical image processing, we often need to deal with a certain kind of image which can be easily segmented into two parts: foreground part and background part. In the background part, the pixel values are all zero. Thus, for this kind of image, we firstly segment the image and denoise and deblur only on the foreground image since there exists no information in the background. Correspondingly, the change of the model is only transferring Ω into Ω/Ω_B where Ω_B represents the background set. In Section 6, we take MR image "Brain" as one example of this kind of image.

3.1. Existence and uniqueness of a solution. We begin with working on the certain condition under which the model is convex before discussing the existence and uniqueness of a solution to (3.3). That is, we will firstly calculate the suitable range of the parameter M which is in the front of the quadratic penalty term.

LEMMA 3.3. *Let* $h(t) = t^{\frac{3}{2}} \frac{(I_0(t)+I_2(t))I_0(t)-2I_1^2(t)}{I_0^2(t)}$, *then* $h(t)$ *is bounded on* $[0, +\infty)$.

Proof. We only need to prove that $\lim_{+\infty} h(t) = 0$. By [35], if $t \in \mathbb{R}$ is large enough, $I_n(t)$ can be written as,

$$I_n(t) = \frac{e^t}{\sqrt{2\pi t}} \left\{ 1 + \sum_{m=1}^{\infty} (-1)^m \frac{(4n^2-1)(4n^2-3^2)...[4n^2-(2m-1)^2]}{m!(8t)^m} \right\}.$$

Taking $n = 0, 1, 2$, we have,

$$\begin{aligned} I_0(t) &= \frac{e^t}{\sqrt{2\pi t}}[1 + \frac{1}{8t} + \frac{9}{128t^2} + \mathcal{O}(\frac{1}{t^3})], \\ I_1(t) &= \frac{e^t}{\sqrt{2\pi t}}[1 - \frac{3}{8t} - \frac{15}{128t^2} + \mathcal{O}(\frac{1}{t^3})], \\ I_2(t) &= \frac{e^t}{\sqrt{2\pi t}}[1 - \frac{15}{8t} + \frac{105}{128t^2} + \mathcal{O}(\frac{1}{t^3})]. \end{aligned}$$

Using the Taylor expansion of $\frac{1}{1+x}$ at $x=0$, readily, we have,

$$
\begin{aligned}
\frac{I_1(t)}{I_0(t)} &= \frac{1-\frac{3}{8t}-\frac{15}{128t^2}+\mathcal{O}(\frac{1}{t^3})}{1+\frac{1}{8t}+\frac{9}{128t^2}+\mathcal{O}(\frac{1}{t^3})} \\
&= \left(1-\frac{3}{8t}-\frac{15}{128t^2}+\mathcal{O}(\frac{1}{t^3})\right)\left(1-(\frac{1}{8t}+\frac{9}{128t^2})+(\frac{1}{8t}+\frac{9}{128t^2})^2+\mathcal{O}(\frac{1}{t^3})\right) \\
&= (1-\frac{3}{8t}-\frac{15}{128t^2})(1-\frac{1}{8t}-\frac{7}{128t^2})+\mathcal{O}(\frac{1}{t^3}) \\
&= 1-\frac{1}{2t}-\frac{1}{8t^2}+\mathcal{O}(\frac{1}{t^3}), \\
\frac{I_2(t)}{I_0(t)} &= (1-\frac{15}{8t}+\frac{105}{128t^2})(1-\frac{1}{8t}-\frac{7}{128t^2})+\mathcal{O}(\frac{1}{t^3}) \\
&= 1-\frac{2}{t}+\frac{1}{t^2}+\mathcal{O}(\frac{1}{t^3}).
\end{aligned}
$$

Further,

$$
\begin{aligned}
(\frac{I_1(t)}{I_0(t)})^2 &= (1-\frac{1}{2t}-\frac{1}{8t^2})^2+\mathcal{O}(\frac{1}{t^3}) \\
&= 1-\frac{1}{t}+\mathcal{O}(\frac{1}{t^3}), \\
\lim_{t\to+\infty} h(t) &= \lim_{t\to+\infty} t^{\frac{3}{2}}\frac{(I_0(t)+I_2(t))I_0(t)-2I_1^2(t)}{I_0^2(t)} \\
&= \lim_{t\to+\infty} t^{\frac{3}{2}}(1+1-\frac{2}{t}+\frac{1}{t^2}-2(1-\frac{1}{t})+\mathcal{O}(\frac{1}{t^3})) \\
&= \lim_{t\to+\infty} t^{\frac{3}{2}}(\frac{1}{t^2}+\mathcal{O}(\frac{1}{t^3})) \\
&= \lim_{t\to+\infty} \frac{1}{\sqrt{t}}+\mathcal{O}(\frac{1}{t^{\frac{3}{2}}}) = 0.
\end{aligned}
$$

Since $h(t)$ is a continuous function on $t\in[0,+\infty)$, the assertion that $h(t)$ is bounded on $[0,+\infty)$ is proved. □

Using the above lemma, let

$$M_0 := \sup_{t\in[0,\infty)} h(t),$$

then M_0 exists. Through numerical computation, readily we can get: when $t=1.81$, $h(t)$ reaches its unique maximum 0.9366 which can be observed in Fig. 3.1.

Proposition 3.4. *If $M \geq M_0$, then the model* (3.3) *is strictly convex.*

Proof. With $t\in\mathbb{R}^+$ and a fixed M, we define a function g as

$$g(t) := -\log I_0(t) - 2M\sqrt{t}.$$

Easily, we have that the second order derivative of g satisfies

$$g''(t) = -\frac{(I_0(t)+I_2(t))I_0(t)-2I_1^2(t)}{2I_0^2(t)}+\frac{M}{2}t^{-\frac{3}{2}}.$$

Straightly, if $M \geq M_0 = \sup t^{\frac{3}{2}}\frac{(I_0(t)+I_2(t))I_0(t)-2I_1^2(t)}{I_0^2(t)}$, we have

$$g''(t) \geq 0.$$

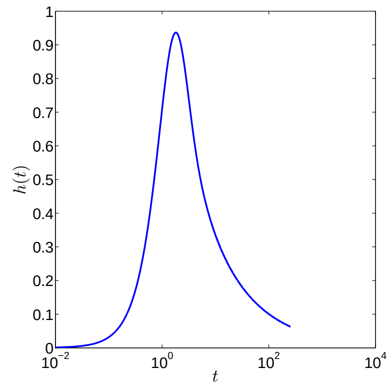

FIG. 3.1. *The range of function value of* $h(t) = t^{\frac{3}{2}} \frac{(I_0(t)+I_2(t))I_0(t)-2I_1^2(t)}{I_0^2(t)}$.

Setting $t = \frac{f(x)u(x)}{\sigma^2}$ for each $x \in \Omega$, we obtain the strict convexity of the first three terms in (3.3). As a prerequisite, the convexity of the TV regularization helps us deduce that model (3.3) is strictly convex, if $M \geq M_0$. Since the feasible set $\bar{S}(\Omega)$ is convex, the assertion is an immediate consequence. $\square$

Based on Proposition 3.4, the following existence and uniqueness results hold.

THEOREM 3.5. *Let f be in $L^\infty(\Omega)$ with $\inf_\Omega f > 0$, then the model (3.3) has a solution u^* in $BV(\Omega)$ satisfying*

$$0 < \frac{M^2\sigma^2}{(2\sup_\Omega f + M\sigma)^2} \inf_\Omega f \leq u^* \leq \sup_\Omega f$$

Moreover, if $M \geq M_0$, the solution of (3.3) is unique.

Proof. Set $c_1 := \frac{M^2\sigma^2}{(2\sup_\Omega f + M\sigma)^2} \inf_\Omega f$, $c_2 = \sup_\Omega f$, and define two functions as follows,

$$E_0(u) = \frac{1}{2\sigma^2}\int_\Omega u^2 dx - \int_\Omega \log I_0(\frac{fu}{\sigma^2})dx + \frac{M}{\sigma}\int_\Omega (\sqrt{u} - \sqrt{f})^2 dx,$$

$$\begin{aligned} E_1(u) &= \frac{1}{2\sigma^2}\int_\Omega u^2 dx - \int_\Omega \log I_0(\frac{fu}{\sigma^2})dx + \frac{M}{\sigma}\int_\Omega (\sqrt{u} - \sqrt{f})^2 dx + \gamma\int_\Omega |Du| dx \\ &= E_0(u) + \gamma\int_\Omega |Du| dx. \end{aligned} \tag{3.4}$$

where $E_1(u)$ is just the objective function in model (3.3).

According to the definition of zero order of Modified Bessel function [9]

$$I_0(x) = \frac{1}{\pi}\int_0^\pi e^{x\cos\theta} d\theta \leq e^x, \qquad \forall x \geq 0, \tag{3.5}$$

we can easily get: for each fixed $x \in \Omega$, $-\log I_0(\frac{f(x)t}{\sigma^2}) \geq -\frac{f(x)t}{\sigma^2}$ with $t \geq 0$. Based on the definition of $E_0(u)$ and $E_1(u)$, we have

$$\begin{aligned} E_1(u) \geq E_0(u) &\geq \frac{1}{2\sigma^2}\int_\Omega u^2 dx - \int_\Omega \log I_0(\frac{fu}{\sigma^2})dx \\ &\geq \int_\Omega (\frac{1}{2\sigma^2}u^2 - \frac{fu}{\sigma^2})dx \\ &= \int_\Omega \frac{(u-f)^2 - f^2}{2\sigma^2}dx \\ &\geq -\frac{1}{2\sigma^2}\int_\Omega f^2 dx. \end{aligned}$$

This means that $E_1(u)$ in (3.3) is bounded from below, thus we can choose a minimizing sequence $\{u_n \in \bar{S}(\Omega) : n = 1, 2, ...\}$.

Since for each fixed $x \in \Omega$, let the real function on $\mathbb{R}^+ \bigcup\{0\}$

$$g(t) := \frac{1}{2\sigma^2}t^2 - \log I_0(\frac{f(x)t}{\sigma^2}) + \frac{M}{\sigma}(\sqrt{t} - \sqrt{f(x)})^2, g'(t) = \frac{1}{\sigma^2}t - \frac{f(x)}{\sigma^2}\frac{I_1(\frac{f(x)t}{\sigma^2})}{I_0(\frac{f(x)t}{\sigma^2})} + \frac{M}{\sigma}(1 - \sqrt{\frac{f(x)}{t}}).$$

Also referred from [9], based on the definition of first order of Modified Bessel function

$$I_1(x) = \frac{1}{\pi}\int_0^\pi \cos\theta e^{x\cos\theta}d\theta, \tag{3.6}$$

we can easily deduce that $-1 \leq \frac{I_1(x)}{I_0(x)} \leq 1$ with $x \geq 0$, combining with the definition of I_0.

Therefore, if $t > f(x)$, we get

$$\begin{aligned} g'(t) &> \frac{1}{\sigma^2}f(x) - \frac{f(x)}{\sigma^2} + \frac{M}{\sigma}(1 - \sqrt{\frac{f(x)}{t}}) \\ &= \frac{M}{\sigma}(1 - \sqrt{\frac{f(x)}{t}}) > 0, \end{aligned}$$

else if $0 \leq t < \frac{M^2\sigma^2}{(2f(x)+M\sigma)^2}f(x) \leq f(x)$,

$$\begin{aligned} g'(t) &< \frac{2f(x)}{\sigma^2} + \frac{M}{\sigma}(1 - \sqrt{\frac{f(x)}{t}}) \\ &\leq \frac{2f(x)}{\sigma^2} + \frac{M}{\sigma}(1 - \frac{2f(x)+M\sigma}{M\sigma}) = 0. \end{aligned}$$

In other word, from the above two inequalities, we know $g(t)$ is increasing if $t \in (f(x), +\infty)$ and decreasing if $0 \leq t < \frac{M^2\sigma^2}{(2f(x)+M\sigma)^2}f(x)$. This implies that $g(\min(t, V)) \leq g(t)$ if $V \geq f(x)$. Furthermore, with $\int_\Omega |D\inf(u, c_2)| \leq \int_\Omega |Du|$ obtained from Lemma 1 in [29], we have

$$E_1(\inf(u, c_2)) \leq E_1(u).$$

Similarly, we can get $E_1(\sup(u, c_1)) \leq E_1(u)$. Hence, we can restrict the minimizing sequence to satisfy $0 < c_1 \leq u_n \leq c_2$, that is, u_n is bounded in $L^1(\Omega)$. Based on the definition of $E_1(u)$, we know $E_1(u_n)$ is bounded. Meanwhile, $\int_\Omega |Du_n|$ is bounded which implies that u_n is bounded in $BV(\Omega)$. Thus, there must exist a subsequence $\{u_{n_k}\}$ which converges strongly in $L^1(\Omega)$ to some $u^* \in BV(\Omega)$, and Du_{n_k} converges weakly to Du^* in the sense of measure. Due to the lower semi-continuity of TV and Fatou's lemma, we can conclude that u^* is a minimizer of problem in (3.3) with restricted condition $0 < c_1 \leq u^* \leq c_2$.

Moreover, if $M \geq M_0$, the problem is strictly convex which implies the uniqueness of the solution. □

Before giving comparison results, we illustrate two lemmas.

LEMMA 3.6. *The function $I_0(x)$ is strictly log-convex for all $x > 0$ where $I_0(x)$ is the Modified Bessel function of first kind of order zero.*

Proof. In order to prove that the function $I_0(x)$ is strictly log-convex in $(0, +\infty)$, it suffices to show that its logarithmic second-order derivative

$$(\log I_0(x))'' = \frac{\frac{1}{2}(I_0(x) + I_2(x))I_0(x) - I_1(x)^2}{I_0^2(x)}$$

is positive in $(0, +\infty)$.
Using (3.5), (3.6) and

$$I_2(x) = \frac{1}{\pi}\int_0^\pi \cos 2\theta e^{x\cos\theta} d\theta,$$

referred from [9], we obtain

$$\begin{aligned}
\frac{1}{2}(I_0(x) + I_2(x))I_0(x) &= \frac{1}{\pi}\int_0^\pi \frac{1+\cos 2\theta}{2} e^{x\cos\theta} d\theta \cdot \frac{1}{\pi}\int_0^\pi e^{x\cos\theta} d\theta \\
&= \frac{1}{\pi}\int_0^\pi \cos^2\theta e^{x\cos\theta} d\theta \cdot \frac{1}{\pi}\int_0^\pi e^{x\cos\theta} d\theta \\
&\geq (\frac{1}{\pi}\int_0^\pi \cos\theta e^{x\cos\theta} d\theta)^2 \\
&= (I_1(x))^2,
\end{aligned}$$

where we have applied Cauchy Schwarz inequality.

Since $\cos\theta e^{\frac{1}{2}x\cos\theta}$ and $e^{\frac{1}{2}x\cos\theta}$ are not linear dependent when θ changes, the equality in above does't hold. Thus, the lemma is finished. □

LEMMA 3.7. *Let $g(x)$ is a strictly convex and strictly increasing function in $(0, +\infty)$. Assume that $0 < a < b$, $0 < c < d$, then we have:*

$$g(ac) + g(bd) > g(ad) + g(bc).$$

Proof. In order to establish the assertion, it suffices to prove that

$$g(bd) - g(bc) > g(ad) - g(ac).$$

Since $g(x)$ is strictly convex in $(0, +\infty)$, $g'(x)$ is strictly increasing in $(0, +\infty)$.
If $bc \geq ad$, then we have

$$\begin{aligned}
g(bd) - g(bc) &\geq g'(bc)b(d-c) \\
&\geq g'(ad)b(d-c) \\
&> g'(ad)a(d-c) \\
&> g(ad) - g(ac).
\end{aligned}$$

If $bc < ad$, then

$$\begin{aligned}
g(bd) - g(bc) &= g(bd) - g(ad) + g(ad) - g(bc) \\
&> g'(ad)d(b-a) + g(ad) - g(bc) \\
&> g'(bc)d(b-a) + g(ad) - g(bc) \\
&> g(bc) - g(ac) + g(ad) - g(bc) \\
&= g(ad) - g(ac).
\end{aligned}$$

Therefore, we complete the proof. $\square$

On the basis of Theorem 3.5, Lemma 3.6 and Lemma 3.7, we can deduce the following comparison principle.

PROPOSITION 3.8. *Let f_1 and f_2 be in $L^\infty(\Omega)$ with $\inf_\Omega f_1 > 0$ and $\inf_\Omega f_2 > 0$. Suppose $u_1^*(resp. u_2^*)$ is a solution of model (3.3) with $f = f_1$ (resp. $f = f_2$). Assume that $f_1 < f_2$, then we have $u_1^* \le u_2^*$ a.e. in Ω.*

Proof. Use the notations $u_1^* \wedge u_2^* = \inf(u_1^*, u_2^*)$, $u_1^* \vee u_2^* = \sup(u_1^*, u_2^*)$. In addition, $E_1^i(u)$ denotes $E_1(u)$ defined in (3.4) with $f = f_i$. Since $u_1^*(resp. u_2^*)$ is a solution of model (3.3) with $f = f_1$ (resp. $f = f_2$), we can easily get

$$E_1^1(u_1^* \wedge u_2^*) \ge E_1^1(u_1^*),$$

$$E_1^2(u_1^* \vee u_2^*) \ge E_1^2(u_2^*).$$

Adding the above two inequalities, and using the fact that $\int_\Omega |D(u_1^* \wedge u_2^*)| + \int_\Omega |D(u_1^* \vee u_2^*)| \le \int_\Omega |Du_1^*| + \int_\Omega |Du_2^*|$, we obtain

$$\begin{aligned}
&\int_\Omega \frac{1}{2\sigma^2}(u_1^* \wedge u_2^*)^2 - \log I_0(\frac{f_1 u_1^* \wedge u_2^*}{\sigma^2}) + \frac{M}{\sigma}(\sqrt{u_1^* \wedge u_2^*} - \sqrt{f_1})^2 dx \\
&\quad + \int_\Omega \frac{1}{2\sigma^2}(u_1^* \vee u_2^*)^2 - \log I_0(\frac{f_2 u_1^* \vee u_2^*}{\sigma^2}) + \frac{M}{\sigma}(\sqrt{u_1^* \wedge u_2^*} - \sqrt{f_2})^2 dx \\
&\qquad \ge \int_\Omega \frac{1}{2\sigma^2}(u_1^*)^2 - \log I_0(\frac{f_1 u_1^*}{\sigma^2}) + \frac{M}{\sigma}(\sqrt{u_1^*} - \sqrt{f_1})^2 dx \\
&\qquad + \int_\Omega \frac{1}{2\sigma^2}(u_2^*)^2 - \log I_0(\frac{f_2 u_2^*}{\sigma^2}) + \frac{M}{\sigma}(\sqrt{u_2^*} - \sqrt{f_2})^2 dx.
\end{aligned} \tag{3.8}$$

As Ω can be written as $\Omega = \{u_1^* > u_2^*\} \cup \{u_1^* \le u_2^*\}$, then we can calculate

$$\int_\Omega ((u_1^* \wedge u_2^*)^2 + (u_1^* \vee u_2^*)^2) dx = \int_\Omega ((u_1^*)^2 + (u_2^*)^2) dx.$$

And the inequality (3.8) can be simplified as follows

$$\int_{\{u_1^* > u_2^*\}} [\log \frac{I_0(\frac{f_1 u_1^*}{\sigma^2}) I_0(\frac{f_2 u_2^*}{\sigma^2})}{I_0(\frac{f_1 u_2^*}{\sigma^2}) I_0(\frac{f_2 u_1^*}{\sigma^2})} + (\sqrt{u_1^*} - \sqrt{u_2^*})(\sqrt{f_1} - \sqrt{f_2})] dx \ge 0. \tag{3.9}$$

Referring to Lemma 3.6 and Lemma 3.7, we can easily get

$$\log I_0(\frac{f_1 u_1^*}{\sigma^2}) + \log I_0(\frac{f_2 u_2^*}{\sigma^2}) < \log I_0(\frac{f_1 u_2^*}{\sigma^2}) + \log I_0(\frac{f_2 u_1^*}{\sigma^2}),$$

which is equivalent to

$$\log \frac{I_0(\frac{f_1 u_1^*}{\sigma^2}) I_0(\frac{f_2 u_2^*}{\sigma^2})}{I_0(\frac{f_1 u_2^*}{\sigma^2}) I_0(\frac{f_2 u_1^*}{\sigma^2})} < 0,$$

if $f_1 < f_2$ and $u_1^* > u_2^*$. Thus, on the basis of the assumption $f_1 < f_2$, we can deduce from inequality (3.9) that $u_1^* > u_2^*$ has zero Lebesgue measure, i.e., $u_1^* \le u_2^*$ a.e. in Ω. ∎

4. The Extension to Simultaneous Deblurring and Denoising. The model (3.3) that we propose is obtained by MAP estimation, and particularly adapt to the Rician noise removal. In this section, we extend it to the case in which we need to deblur and denoise simultaneously. That is, we will recover the image u in (1.1) with the blurring operator A. The restoration is conducted by solving the following minimization problem

$$\inf_{u\in \bar{S}(\Omega)} \frac{1}{2\sigma^2}\int_\Omega (Au)^2 dx - \int_\Omega \log I_0(\frac{Auf}{\sigma^2})dx + \frac{M}{\sigma}\int_\Omega (\sqrt{Au} - \sqrt{f})^2 dx + \gamma \mathrm{TV}(u), \quad (4.1)$$

where $A \in \mathcal{L}(L^2(\Omega))$. As a blurring operator, we assume that A is nonnegative, i.e., $A \ge 0$ in short. Then we have $Au \ge 0$ with $u \in \bar{S}(\Omega)$.

Since A is linear, based on Proposition 3.4 and Theorem 3.5, we can easily obtain the following results.

PROPOSITION 4.1. *If $M \ge M_0$, then the model* (4.1) *is convex.*

THEOREM 4.2. *Assume that $A \in \pounds(L^2(\Omega))$ is nonnegative, and it does not annihilate constant functions, i.e., $A1 \neq 0$. Let f be in $L^\infty(\Omega)$ with $\inf_\Omega f > 0$, then the model* (4.1) *has a solution u^*. Moreover, if $M \ge M_0$ and A is injective, then the solution is unique.*

Proof. Define one function $E_A(u)$ as follows

$$E_A(u) = \frac{1}{2\sigma^2}\int_\Omega (Au)^2 dx - \int_\Omega \log I_0(\frac{Auf}{\sigma^2})dx + \frac{M}{\sigma}\int_\Omega (\sqrt{Au} - \sqrt{f})^2 dx + \gamma \int_\Omega |Du| dx.$$

Similar as in the proof of Theorem 3.5 , E_A is bounded from below. Thus, we choose a minimizing sequence $\{u_n \in \bar{S}(\Omega) : n = 1, 2, \ldots\}$ for (4.1), and have $\{\int_\Omega |Du_n|\}$ is bounded. Applying the Poincaré inequality in [33], we get

$$\|u_n - m_\Omega(u_n)\|_2 \le C\int_\Omega |D(u_n - m_\Omega(u_n))| = C\int_\Omega |Du_n|, \quad (4.2)$$

where $m_\Omega(u_n) = \frac{1}{|\Omega|}\int_\Omega u_n \, dx$, $|\Omega|$ denotes the measure of Ω, and C is a constant. As Ω is bounded, $\|u_n - m_\Omega(u_n)\|_2$ is bounded for each n. Since $A \in \mathcal{L}(L^2(\Omega))$ is continuous, $\{A(u_n - m_\Omega(u_n))\}$ must be bounded in $L^2(\Omega)$ and in $L^1(\Omega)$.

In addition, based on the boundedness of $E_A(u_n)$, $\|\sqrt{Au_n} - \sqrt{f}\|^2$ is bounded, which deduces that Au_n is bounded in $L^1(\Omega)$. Meanwhile, we have:

$$|m_\Omega(u_n)| \cdot \|A1\|_1 = \|A(u_n - m_\Omega(u_n)) - Au_n\|_1 \le \|A(u_n - m_\Omega(u_n))\|_1 + \|Au_n\|_1,$$

which turns out that $m_\Omega(u_n)$ is uniformly bounded, because of $A1 \neq 0$. As we know $\{u_n - m_\Omega(u_n)\}$ is bounded, the boundedness of $\{u_n\}$ in $L^2(\Omega)$ and thus in $L^1(\Omega)$ is obvious.

Therefore, there exists a subsequence $\{u_{n_k}\}$ which converges weakly in $L^2(\Omega)$ to some $u^* \in L^2(\Omega)$, and $\{Du_{n_k}\}$ converges weakly as a measure to Du^*. Since the linear operator A is continuous, we have $\{Au_{n_k}\}$ converges weakly to Au^* in $L^2(\Omega)$ as well. Then according to the lower semi-continuity of the total variation and Fatou's lemma, we obtain that u^* is a solution of the model (4.1).

Based on Theorem 3.5, when $M \geq M_0$, the model (4.1) is convex. Furthermore, if A is injective, (4.1) is strictly convex, then its minimizer has to be unique. ∎

5. Primal-Dual Algorithm. As model (3.3) is convex when $M \geq M_0$, many optimization methods can be applied to solve the minimization problem in (3.3). For instance, Split-Bregman method [27] is widely used in this case because of its many superiorities, such as small memory footprint, easy to code; gradient method is also a suitable classical method to solve this optimization problem and so on. In particular, we introduce the primal-dual method [14] since it is easy to implement and can be effectively accelerated on parallel hardware such as graphics processing units (GPUs). Moreover, it is built with the convergence theories.

We write the model (3.3) as the following discrete formula

$$\min_{u\in X} \frac{1}{2\sigma^2}\|u\|_2^2 - \langle \log I_0(\frac{fu}{\sigma^2}), 1\rangle + \frac{M}{\sigma}\|\sqrt{u} - \sqrt{f}\|_2^2 + \gamma\|\nabla u\|_1, \tag{5.1}$$

where $X = \{v \in \mathbb{R}^n : v_i \geq 0 \text{ for } \; i = 1, \cdots, n\}$, $f \in X$ is columnwise stacked into a vector from a 2D pixel-array, $\|\cdot\|_2$ denotes the l^2-vector norm, $\langle u, v\rangle = \sum_{i=1}^n u_i v_i$ is the vector inner product, and n is the number of pixels in the image. Furthermore, $\|\nabla u\|_1$ denotes the discrete version of the isotropic total variation, which is defined as $\|\nabla u\|_1 = \sum_{i=1}^n \sqrt{(\nabla_x u)_i^2 + (\nabla_y u)_i^2}$ with $\nabla u = (\nabla_x u, \nabla_y u)^\top \in \mathbb{R}^{2n}$, and symmetric boundary conditions are used for the discrete gradient operator ∇.

In order to give a brief expression, we denote the sum of the first three terms in (5.1) as the function $G : X \to \mathbb{R}$, that is,

$$G(u) := \frac{1}{2\sigma^2}\|u\|_2^2 - \langle \log I_0(\frac{fu}{\sigma^2}), 1\rangle + \frac{M}{\sigma}\|\sqrt{u} - \sqrt{f}\|_2^2.$$

According to the duality of the TV, the primal-dual formulation of the optimization problem in (5.1) is given by

$$\max_{p\in Y}\min_{u\in X} G(u) - \gamma\langle u, \operatorname{div} p\rangle, \tag{5.2}$$

where $Y = \{q \in \mathbb{R}^{2n} : \|q\|_\infty \leq 1\}$, $\|q\|_\infty = \max_{i\in\{1,\cdots,n\}} \left|\sqrt{q_i^2 + q_{i+n}^2}\right|$ denotes the l^∞-vector-norm, p is the dual variable, and the divergence operator $\operatorname{div} = -\nabla^\top$. The algorithm is summarized as follows.

Algorithm for solving the model (3.3)

1: Fixed α, γ, σ, β, and τ. Initialize $u^0 = f$, $\bar{u}^0 = f$, and $p^0 = (0, \cdots, 0)^\top \in \mathbb{R}^{2n}$.

2: Calculate p^{k+1} and u^{k+1} from

$$\begin{aligned} p^{k+1} &= \arg\max_{p\in Y} \gamma\langle \nabla \bar{u}^k, p\rangle - \frac{1}{2\beta}\|p - p^k\|_2^2 \\ &= \pi_1(\beta\gamma\nabla\bar{u}^k + p^k), \end{aligned} \tag{5.3}$$

$$u^{k+1} = \arg\min_{u\in X} G(u) - \gamma\langle u, \operatorname{div} p^{k+1}\rangle + \frac{1}{2\tau}\|u - u^k\|_2^2, \tag{5.4}$$

$$\bar{u}^{k+1} = 2u^{k+1} - u^k, \tag{5.5}$$

where π_1 is the projector onto the l^2-normed unit ball, i. e.,

$$\pi_1(q_i) = \frac{q_i}{\max\{1, |q_i|\}} \text{ and } \pi_1(q_{n+i}) = \frac{q_{n+i}}{\max\{1, |q_i|\}}, \text{ for } \; i = 1, \cdots, n,$$

with $|q_i| = \sqrt{q_i^2 + q_{n+i}^2}$.

3: Stop; or set $k := k + 1$ and go to step 2.

In the algorithm, we utilize Newton method to solve the minimization problem in (5.4) because of the strict convexity of our proposed model. In addition, based on Theorem 1 in [13], we have the following convergence result.

PROPOSITION 5.1. *The iterates* (u^k, p^k) *of our algorithm converge to a saddle point of* (3.3)*, provided that* $\beta\tau\gamma^2\|\nabla\|^2 < 1$.

According to the result $\|\nabla\|^2 \leq 8$ with the unit spacing size between pixels in [13], we only need $\beta\tau\gamma^2 < \frac{1}{8}$ in order to keep the convergent condition. While, in our numerical practice, γ is tuned empirically, and we set $\beta = 0.8/\gamma, \tau = 0.2/\gamma$, which already can ensure the convergence of the algorithm.

In order to extend the primal-dual algorithm to solve deblurring model (4.1), we introduce another two variables. Based on the definition of TV, (4.1) can be written as

$$\max_{p\in Y, q\in Z} \min_{u\in X, w\in X} G(w) - \gamma\langle u, \operatorname{div} p\rangle + \langle Au - w, q\rangle,$$

where w is the approximation of Au, and $q \in Z = \{v \in \mathbb{R}^n : v_i \geq 0, i = 1, ..., n\}$ is the Lagrangian multiplier of the constraint $Au = w$. The resulting algorithm is summarized as follows.

Algorithm for solving the model (4.1)

1: Fixed α, γ, σ, τ, and β. Initialize $u^0 = f$, $\bar{u}^0 = f$, $w^0 = f$, $\bar{w}^0 = f$, $p^0 = (0, \cdots, 0)^\top \in \mathbb{R}^{2n}$, and $q^0 = (0, \cdots, 0) \in \mathbb{R}^n$.

2: Calculate p^{k+1}, q^{k+1}, w^{k+1} and u^{k+1} from

$$p^{k+1} = \arg\max_{p\in Y} \langle \gamma\nabla\bar{u}^k, p\rangle - \frac{1}{2\beta}\|p - p^k\|_2^2, \tag{5.6}$$

$$q^{k+1} = \arg\max_{q\in Z} \langle A\bar{u}^k - \bar{w}^k, q\rangle - \frac{1}{2\beta}\|q - q^k\|_2^2, \tag{5.7}$$

$$u^{k+1} = \arg\min_{u\in X} \langle u, A^\top q^{k+1} - \gamma \operatorname{div} p^{k+1}\rangle + \frac{1}{2\tau}\|u - u^k\|_2^2, \tag{5.8}$$

$$w^{k+1} = \arg\min_{w\in X} G(w) - \langle w, q^{k+1}\rangle + \frac{1}{2\tau}\|w - w^k\|_2^2, \tag{5.9}$$

$$\overline{u}^{k+1} = 2u^{k+1} - u^k, \tag{5.10}$$

$$\overline{w}^{k+1} = 2w^{k+1} - w^k, \tag{5.11}$$

3: Stop; or set $k := k + 1$ and go to step 2.

Based on the Proposition 4.2 and Proposition 4.3 in [18], we end this section by the convergence properties of the algorithm for solving (4.1).

PROPOSITION 5.2. *Let* $x = (u, w)^\top$ *and* $y = (p, q)^\top$. *If we choose* τ *and* β *such that* $\tau\beta \leq 1/(1 + \gamma^2\|\nabla\|_2^2 + \|A\|_2^2)$*, then the iterates* (x^k, y^k) *converge to a saddle point* (x^*, y^*) *of* (4.1).

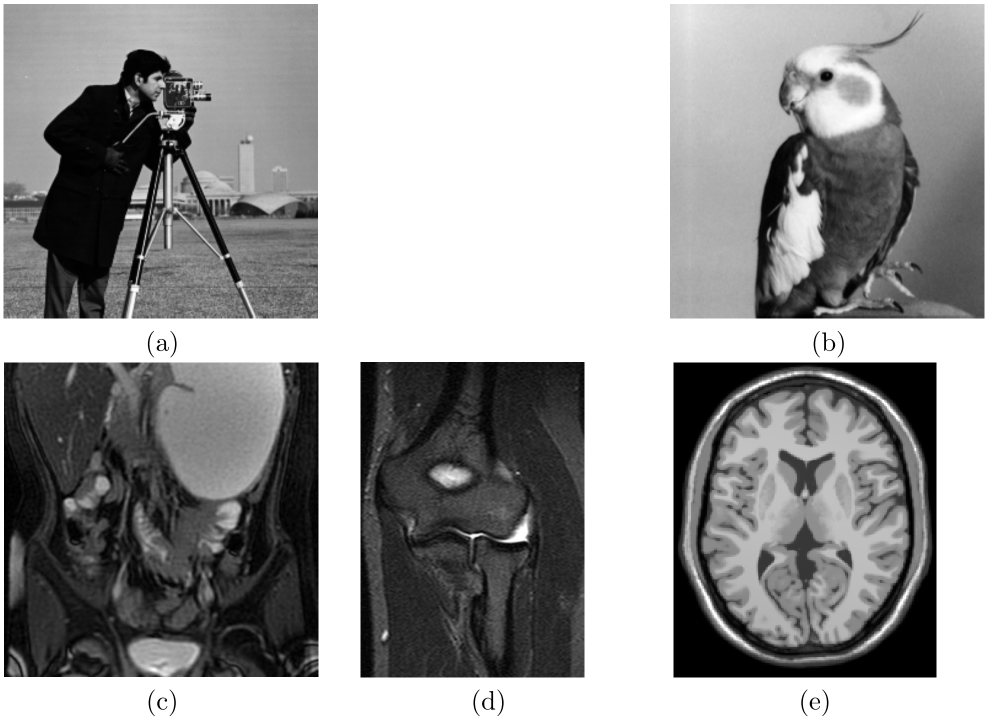

Fig. 6.1. *Original images. (a) "Cameraman", (b) "Bird", (c) "Skull", (d) "Leg joint", (e) "Brain".*

6. Numerical Results. In this section, we report some numerical results to illustrate the effectiveness of our proposed approach. In total, we use five images for testing: two natural images "Cameraman" and "Bird", and three MR images "Skull", "Leg joint" and "Brain", see Fig. 6.1. We compare our proposed approach with the classical ROF model [36] and Getreuer's convex model in [26], and both of them are efficient for image recovery. The ROF model is solved by the primal-dual algorithm, and can be served as reference since it doest not consider the characteristics of the noise. The Getreuer's model is based on MAP estimation taking full account of the distribution of the Rician noise, and is solved by the Split-Bregman algorithm [27]. In the numerical experiments, we observe a phenomenon that there exists rather big gap between the mean of the restored image by our model (or ROF model) and that of the original image. In order to compensate the gap, we make a bias correction step in the end. Indeed, based on (1.1), we can easily get

$$Au = -\eta_1 + \sqrt{f^2 - \eta_2^2}.$$

Hence,

$$\mathbb{E}(u) \approx \mathbb{E}(Au) = \mathbb{E}(\sqrt{f^2 - \eta_2^2}) \approx \mathbb{E}(\sqrt{\max(f^2 - c\sigma^2, 0)}),$$

where the constant c should be nearly 1.

Under independence conditions, the above approximations are theoretically resonable in statistics. Moreover, in the practical simulations, we find that these two assumptions provide rather good results. Assuming that u is the resulting image of our model or ROF model, the above analysis suggests that we could revise it as

$$\hat{u} = u + a,$$

where a is the mean value of the difference between u and $\sqrt{\max(f^2 - c\sigma^2, 0)}$. In our paper, we choose $c = 1.2$ and list relative estimation errors of three images as examples in Table 6.1. From Table 6.1, we can see that the estimated results are quite good. For the Getreuer's model, we numerically find that this bias correction is not necessary.

	Relative Estimation Error for different σ			
images	$\sigma = 15$	$\sigma = 20$	$\sigma = 25$	$\sigma = 30$
Cameraman	0.0009	0.0044	0.0071	0.0105
Skull	0.0107	0.0054	0.0154	0.0265
Leg joint	0.0043	0.0108	0.0081	0.0027

TABLE 6.1

The values of $\frac{|A_{esti} - A_{true}|}{A_{true}}$ *for different Rician noise standard variation* σ *with different image* u*, where* A_{esti} *denotes the estimated mean value of* u*, while* A_{true} *denotes the true mean value of* u*.*

For all the three image restoration methods used in this section, we tuned the parameters in the experiments to achieve the best visual results. For the quality of the restoration results, we measure it quantitatively by the Peak-Signal-to-Noise Ratio (PSNR) [28] value which is commonly used in image processing. All the experiments are executed on a ACPI×64-based PC with 3.3GHz CPU and Matlab 7.12.0 (R2011a).

6.1. Image denoising. In the denoising case, the test images are degraded by Rician noise with standard deviation $\sigma = 20$ and $\sigma = 30$, respectively. In our model, we fix $M = 0.94$ which ensures the convexity of our model (3.3). As the stopping criteria for the algorithm used by three different models, we design it as

$$\frac{\|u^k - u^{k+1}\|_2}{\|u^{k+1}\|_2} < \epsilon, \tag{6.1}$$

where ϵ is set by 10^{-4}.

In Fig. 6.2, we present the restored images by our proposed model, ROF model and Getreuer's model from the "Cameraman" image degraded by Rician noise with $\sigma = 20$. From Fig. 6.2, we can see that the noisy "Cameraman" image is enhanced by all the three models. Compared with the other two models, ROF model smooths the image more damnably which is also re-confirmed in the residual image and lowest PSNR value in Table 6.2. However, the contrast of the resulting image of Getreuer's model seems worst, for example, the intensity of the trousers of the cameraman is much lighter than the original one. The image recovered by our proposed model preserves most feature while clearly removing the noise. From the information in the yellow rectangle of Fig. 6.2, we can see that the hand of our recovered image contains most details. In Fig. 6.3, we show the residual images of "Leg joint" obtained by three models. We can find that the residual image of our model contains least information of the observed image, in addition, some particular positions in the residual part of Getreuer's model are especially brighter than those in our proposed model. In general,

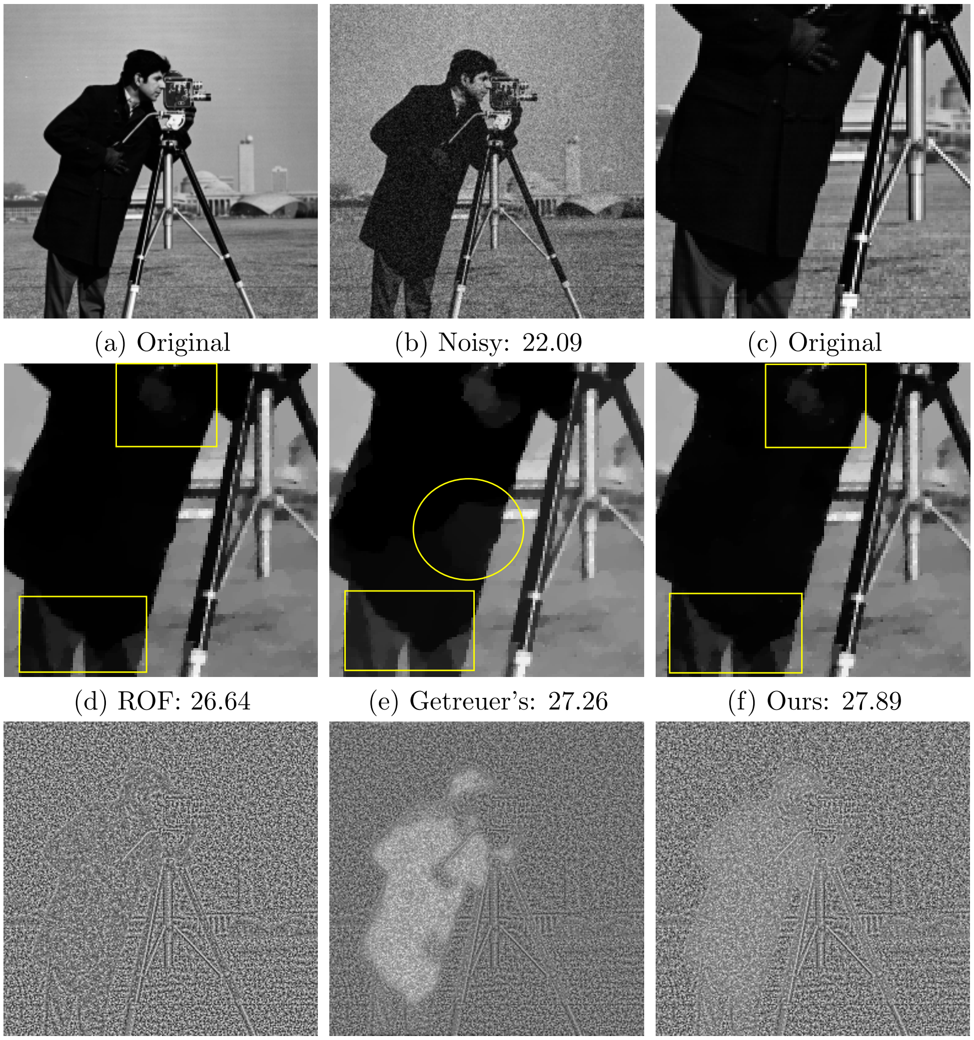

(a) Original (b) Noisy: 22.09 (c) Original

(d) ROF: 26.64 (e) Getreuer's: 27.26 (f) Ours: 27.89

(g) Residual of ROF (h) Residual of Gretreuer (i) Residual of Ours

FIG. 6.2. *Results and PSNR values of different methods when removing the Rician noise with $\sigma = 20$ in natural image "Cameraman". Row 1: the original image "Cameraman" and the degraded image. Row 2: the recovered images with different methods. Row 3: the residuals images with different methods. (a) Original "Cameraman", (b) Noisy "Cameraman" with $\sigma = 20$, (c) Zoomed original "Cameraman", (d) ROF model ($\lambda = 0.05$), (e) Getreuer's model ($\lambda = 20$), (f) Our proposed model ($\gamma = 0.05$), (g)-(i) are residual images of ROF model, Getreuer's model and our model, respectively.*

the reconstructed image by our proposed model performs best visually. In numerical aspect, the whole three models are monotonically decreasing. Simultaneously, the PSNR value of our model is largest according to Table 6.2. Note that the PSNR values listed in Table 6.2 are the best PSNR values obtained by three models through adjusting the parameters to remove noise. The corresponding parameters are given in the captions of Fig. 6.2-6.5.

From Table 6.2, it is easily found that the larger the standard variance σ of Rician noise is, the improvement of our method over the other two approaches seems more

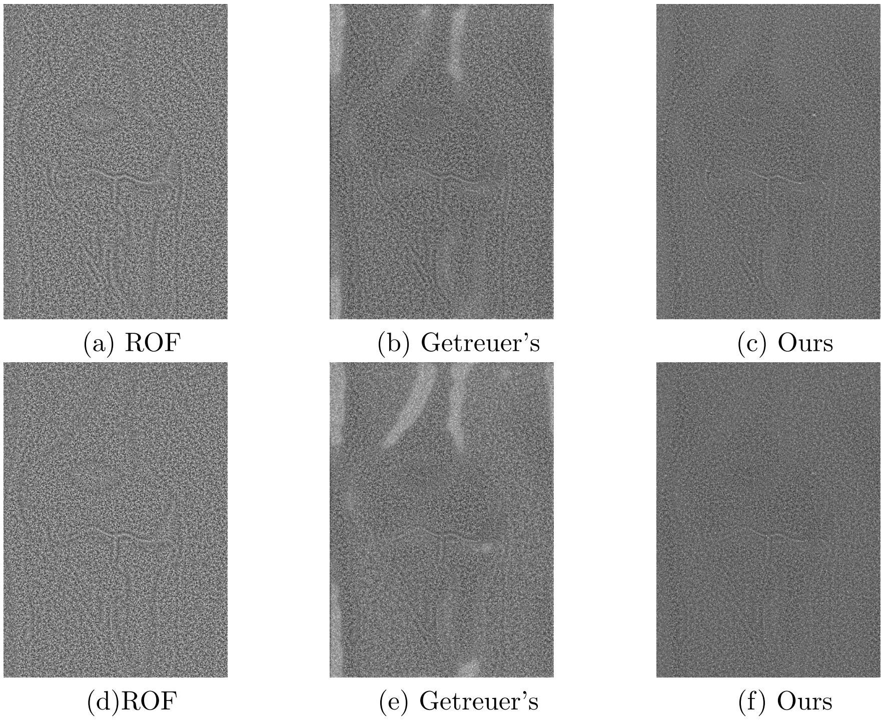

FIG. 6.3. *Residual images of different methods when removing the Rician noise with $\sigma = 20$ and $\sigma = 30$ in MR image "Leg joint". Row 1: The $\sigma = 20$ case; Row 2: The $\sigma = 30$ case; (a) and (d) are obtained by ROF model; (b) and (e) are obtained by Getreuer's model; (c) and (f) are obtained by our proposed model.*

significant. In order to show the superiority of our proposed model, we also present the restored results of natural image "Bird" and MR image "Brain" in Fig. 6.4-6.5. The corresponding PSNR values obtained by all the three models are listed in Table 6.2.

In Fig. 6.4, we provide a visual comparison of a slice of the natural image (Bird) denoised using three methods. Note that the noisy image is degraded by Rician noise with standard variation $\sigma = 30$. Our method is seen to provide most details of the image. For example, the paws of the bird in our image is clearest. In Fig. 6.5, we zoom in to the restored "Brain" images by above-mentioned three methods to get more detail. The conclusion is easily obtained that image reconstructed by our method preserves most detail information among three images.

6.2. Image deblurring and denoising. In Section 6.1, we discuss to recover the noisy images. Since we have already extended the noisy case to the simultaneous blurred with noise one in Section 4, in this section, we consider restoring the noisy blurred images. For the blurring operators, two kinds of blurring operators are applied. One is Gaussian blur with a window size $9 * 9$ and standard deviation 1, the other one is Motion blur with length 5 and angle 30. In the experiment, after blurred, the test images are degraded by Rician noise with $\sigma = 15$. In the deblurring case, the stopping criteria ϵ is set by 10^{-4}.

In Fig. 6.6-6.7, we show the degraded images and the recovered results by solving three models : ROF model, Getreuer's and ours. In this deblurring case, we select

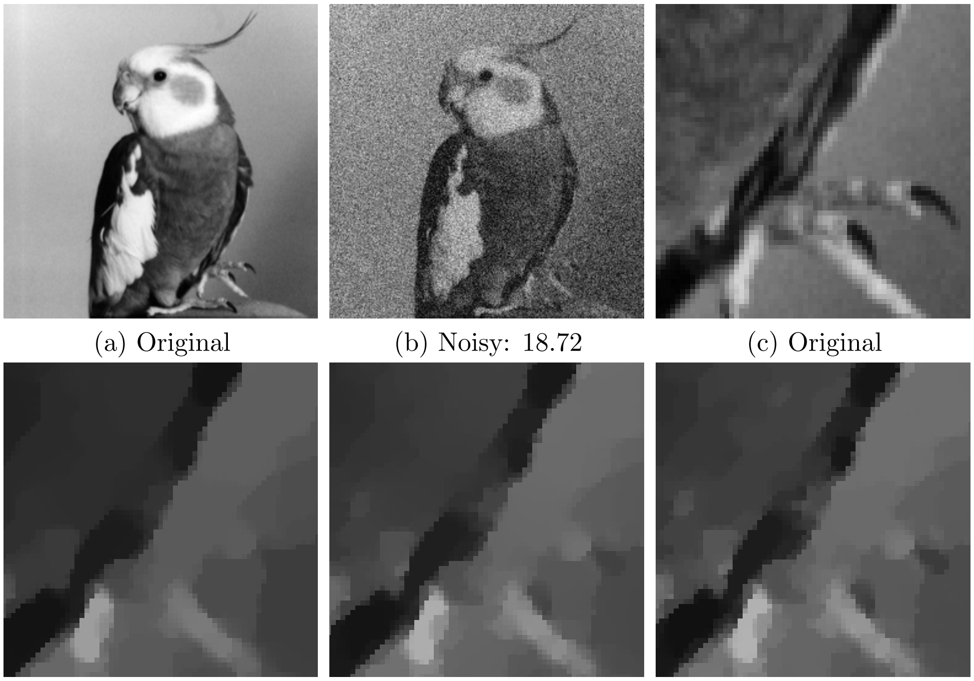

(a) Original (b) Noisy: 18.72 (c) Original

(d) ROF: 28.03 (e) Getreuer's: 30.09 (f) Ours: 30.62

FIG. 6.4. *Results and PSNR values of different methods when removing the Rician noise with $\sigma = 30$ in natural image "Bird". Row 1: the original image "Bird" and the degraded image. Row 2: the recovered images with different methods. (a) Original "Bird", (b) Noisy "Bird" with $\sigma = 30$, (c) Zoomed original "Bird", (d) ROF model ($\lambda = 0.03$), (e) Getreuer's model ($\lambda = 30$), (f) Our proposed model ($\gamma = 0.035$).*

to present the restored results of two images (one natural image "Bird" and one MR image "Brain"). In Table 6.3, we list the best PSNR values obtained by three models for both Gaussian blur and Motion blur. From Table 6.3, we can see that in this deblurring case, the PSNR values gotten by our model are still best and the PSNR values obtained by ROF model are quite good. This phenomenon matches the opinion proposed in [2, 7] that when the standard deviation σ of the Rician noise is not so large, it can be well approximated by Gaussian noise. Since in the deblurring case, σ is set by 15, the result by ROF model can be very good. From Fig. 6.6-6.7, we can easily find that our model performs best in removing the noise clearly.

In Fig. 6.6, the background of the reconstructed image by our model is more similar to the original image "Bird" than the other two models. Our method produces least artifacts, at the same time, it is able to provide better preservation of edges and other details. In Fig. 6.7, we list the residual images of three methods. The residual image of our method contains least information of the original "Brain" image which means our method is able to best preserve the features of the original image. Meanwhile, we can get the same conclusion from the PSNR values listed in Table 6.3.

In a conclusion, our model outperforms the other two models which can deblur with removing Rician noise simultaneously.

7. Conclusion. In this paper, we put forward a new convex variational model for recovering blurred images with Rician noise. Taking account of the statistical

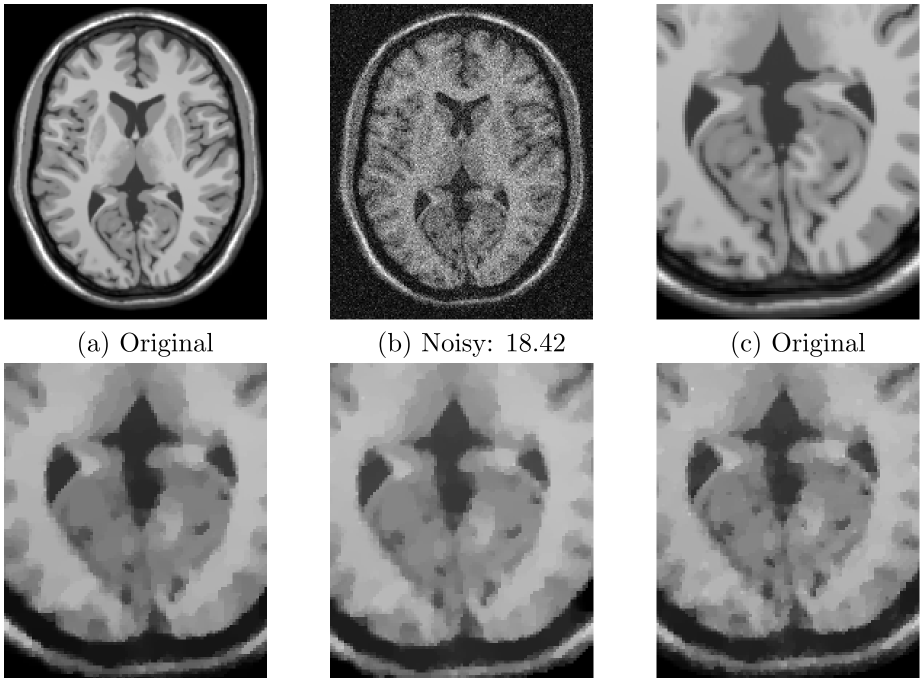

(a) Original (b) Noisy: 18.42 (c) Original

(d) ROF: 22.50 (e) Getreuer's: 25.71 (f) Ours: 26.52

Fig. 6.5. *Results and PSNR values of different methods when removing the Rician noise with* $\sigma = 30$ *in MR image "Brain". Row 1: the original image "Brain" and the degraded image. Row 2: the recovered images with different methods. (a) Original "Brain", (b) Noisy "Brain" with* $\sigma = 30$*, (c) Zoomed original "Brain", (d) ROF model (*$\lambda = 0.03$*), (e) Getreuer's model (*$\lambda = 30$*), (f) Our proposed model (*$\gamma = 0.03$*).*

property of Rician noise, we eventually come up with adding a quadratic penalty term into the non-convex model (1.2) obtained by MAP estimation to establish a new convex model (3.3). The new model can guarantee the uniqueness of the solution and the stability of the algorithm. Moreover, based on the convexity of the new model (3.3), primal-dual algorithm presented in [14] is applied to solve it since the convergence is ensured. Furthermore, experimental results presented in the end show that our proposed method can restore the degraded image by Rician noise effectively.

REFERENCES

[1] M. Abramowitz and I. A Stegun, *Handbook of mathematical functions with formulas, graphs, and mathematical tables. national bureau of standards applied mathematics series 55. tenth printing.*, (1972).

[2] J. Aelterman, B. Goossens, A. Pizurica, and W. Philips, *Removal of correlated rician noise in magnetic resonance imaging*, in Proceedings of EUSIPCO, vol. 2008, 2008.

[3] L. Ambrosio, N. Fusco, and D. Pallara, *Functions of Bounded Variation and Free Discontinuity Problem*, Oxford university press, 2000.

[4] G. Aubert and J.-F. Aujol, *A variational approach to removing multiplicative noise*, SIAM J. Appl. Math., 68 (2008), pp. 925–946.

[5] G. Aubert and P. Kornprobst, *Mathematical Problems in Image Processing: Partial Differential Equations and the Calculus of Variations*, vol. 147, Springer, 2006.

[6] E. Bae, J. Yuan, and X. Tai, *Global minimization for continuous multiphase partitioning problems using a dual approach*, Int. J. Comput Vis., 92 (2011), pp. 112–129.

		$\sigma = 20$	$\sigma = 30$
Images	Models	PSNR(dB)	PSNR(dB)
	Noisy	22.09	18.46
	ROF	26.64	23.61
Cameraman	Getreuer's	27.26	25.10
	Ours	**27.97**	**25.81**
	Noisy	22.21	18.72
	ROF	31.55	28.03
Bird	Getreuer's	32.39	30.09
	Ours	**32.87**	**30.62**
	Noisy	22.11	18.53
	ROF	28.22	25.28
Skull	Getreuer's	29.39	26.40
	Ours	**29.89**	**27.89**
	Noisy	22.31	18.83
	ROF	30.08	28.06
Leg joint	Getreuer's	31.10	28.93
	Ours	**31.57**	**29.34**
	Noisy	21.87	18.42
	ROF	25.82	22.50
Brain	Getreuer's	28.16	25.71
	Ours	**28.60**	**26.52**
	Noisy	21.92	18.59
	ROF	28.46	25.50
Average	Getreuer's	29.66	27.25
	Ours	**30.18**	**28.04**

Table 6.2

The comparisons of PSNR values by different methods for denoising case with $\sigma = 20$ and $\sigma = 30$, respectively.

[7] P. Bao and L. Zhang, *Noise reduction for magnetic resonance images via adaptive multiscale products thresholding*, IEEE Trans. Med. Imaging, 22 (2003), pp. 1089–1099.

[8] S. Basu, T. Fletcher, and R. Whitaker, *Rician noise removal in diffusion tensor mri*, Medical Image Computing and Computer-Assisted Intervention–MICCAI 2006, (2006), pp. 117–125.

[9] F. Bowman, *Introduction to Bessel functions*, DoverPublications. com, 1958.

[10] A. Buades, B. Coll and J. Morel, *A non-local algorithm for image denoising*, In: IEEE Conf. on CVPR, 2 (2005), pp. 60–65.

[11] J. Cai, R. Chan, and M. Nikolova, *Two-phase approach for deblurring images corrupted by impulse plus gaussian noise*, Inverse Problems and Imaging, 2 (2008), pp. 187–204.

[12] J. Cai, B. Dong, S. Osher, and Z. Shen, *Image restoration: Total variation, wavelet frames, and beyond*, J. Amer. Math. Soc., 25 (2012), pp. 1033–1089.

[13] A. Chambolle, *An algorithm for total variation minimization and applications*, J. Math. Imaging Vision, 20 (2004), pp. 89–97.

[14] A. Chambolle and T. Pock, *A first-order primal-dual algorithm for convex problems with applications to imaging*, J. Math. Imaging Vision, 40 (2011), pp. 120–145.

[15] T. Chan and J. Shen, Image Processing And Analysis: Variational, PDE, Wavelet, And Stochastic Methods, SIAM Publisher, 2005.

[16] R. Chan, T. Chan, and A. Yip, *Numerical methods and applications in total variation image restoration*, Handbook of Mathematical Methods in Imaging, (2011), pp. 1059–1094.

[17] R. Chan and Chen. K, *Fast multigrid algorithm for a minimization problem in impulse noise removal*, SIAM J. Sci. Comput., 30 (2008), pp. 1474–1489.

[18] R. Chan, H. Yang, and T. Zeng, *A two-stage image segmentation method for blurry images*

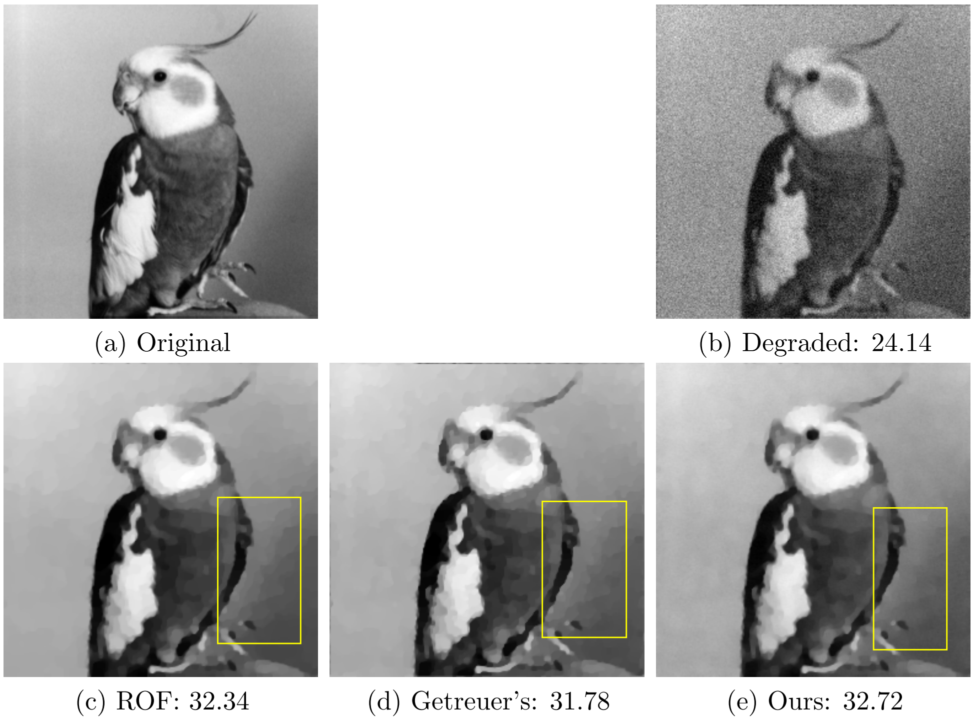

Fig. 6.6. *Results and PSNR values of different methods when restoring the degraded images corrupted by Gaussian blur and then Rician noise with $\sigma = 15$. Row 1: Original image and degraded image. Row 2 : recovered images with different methods. (a) Original "Bird", (b) degraded "Bird", (c) ROF model ($\lambda = 0.2$), (d) Vese model ($\lambda = 30$;), (e) our method ($\gamma = 0.05$)*

with poisson or multiplicative gamma noise, CAM report 13-30, (2013).

[19] T. Chan and J. Shen, *Image Processing And Analysis: Variational, Pde, Wavelet, And Stochastic Methods*, SIAM, 2005.

[20] H. Chen, J. Song, and X. Tai, *A dual algorithm for minimization of the llt model*, Adv. Comput. Math., 31 (2009), pp. 115–130.

[21] P. Coupé, P. Yger, S. Prima, P. Hellier, C. Kervrann, and C. Barillot, *An optimized blockwise nonlocal means denoising filter for 3-d magnetic resonance images*, IEEE Trans. Med. Imaging, 27 (2008), pp. 425–441.

[22] Y. Dong, M. Hintermuller, and M. Ner, *An efficient primal-dual method for l1-tv image restoration*, SIAM J. Imaging Sci., 2 (2009), pp. 1168–1189.

[23] Y. Dong and T. Zeng, *A convex variational model for restoring blurred images with multiplicative noise*, SIAM J. Imaging Sci., 6 (2013), pp. 1598–1625.

[24] M. Elad and M. Aharon, *Image denoising via sparse and redundant representations over learned dictionaries*, IEEE Trans. Image Process., 15 (2006), pp. 3736–3745.

[25] G. Gerig, O. Kubler, R. Kikinis, and F. A Jolesz, *Nonlinear anisotropic filtering of mri data*, IEEE Trans. Med. Imaging, 11 (1992), pp. 221–232.

[26] P. Getreuer, M. Tong, and L. Vese, *A variational model for the restoration of mr images corrupted by blur and rician noise*, Advances in Visual Computing, (2011), pp. 686–698.

[27] T. Goldstein and S. Osher, *The split bregman method for l1-regularized problems*, SIAM J. Imaging Sci., 2 (2009), pp. 323–343.

[28] A. Hore and D. Ziou, *Image quality metrics: Psnr vs. ssim*, in Pattern Recognition (ICPR), 2010 20th International Conference on, IEEE, 2010, pp. 2366–2369.

[29] P. Kornprobst, R. Deriche, and G. Aubert, *Image sequence analysis via partial differential equations*, J. Math. Imaging Vision, 11 (1999), pp. 5–26.

[30] T. Le, R. Chartrand, and T. Asaki, *A variational approach to reconstructing images corrupted by poisson noise*, J. Math. Imaging Vision, 27 (2007), pp. 257–263.

[31] J. Manjón, N. A Thacker, J. J Lull, G. Garcia-Martí, L. Martí-Bonmatí, and M. Rob-

		Gaussian Blur	Motion Blur
Images	Models	PSNR(dB)	PSNR(dB)
Cameraman	Degraded	22.22	21.66
	ROF	25.34	24.39
	Getreuer's	25.47	24.61
	Ours	**25.87**	**25.01**
Bird	Degraded	24.14	23.97
	ROF	32.34	31.95
	Getreuer's	31.78	31.49
	Ours	**32.72**	**32.21**
Skull	Degraded	24.34	24.15
	ROF	30.42	29.57
	Getreuer's	30.56	29.95
	Ours	**31.15**	**30.64**
Leg joint	Degraded	24.49	24.42
	ROF	31.30	31.12
	Getreuer's	31.67	31.46
	Ours	**32.07**	**31.86**
Brain	Degraded	22.67	22.28
	ROF	25.72	25.12
	Getreuer's	27.25	26.29
	Ours	**27.90**	**27.05**
Average	Degraded	23.57	23.30
	ROF	29.02	28.43
	Getreuer's	29.35	28.76
	Ours	**29.94**	**29.35**

TABLE 6.3

The comparisons of PSNR values by different methods for deblurring and denoising case for Gaussian Blur and Motion Blur with Rician noise $\sigma = 15$, respectively.

LES, *Multicomponent mr image denoising*, Journal of Biomedical Imaging, 2009 (2009), p. 18.

[32] R. D NOWAK, *Wavelet-based rician noise removal for magnetic resonance imaging*, IEEE Trans. Image Process, 8 (1999), pp. 1408–1419.

[33] L. E PAYNE AND H. F WEINBERGER, *An optimal poincaré inequality for convex domains*, Arch. Ration. Mech. Anal., 5 (1960), pp. 286–292.

[34] P. PERONA AND J. MALIK, *Scale-space and edge detection using anisotropic diffusion*, IEEE Trans. Pattern Anal. Mach. Intell., 12 (1990), pp. 629–639.

[35] A. D POLIANIN AND ZAĬ, *Handbook of exact solutions for ordinary differential equations*.

[36] L. RUDIN, S. OSHER, AND E. FATEMI, *Nonlinear total variation based noise removal algorithms*, Physica D, 60 (1992), pp. 259–268.

[37] N. WIEST-DAESSLÉ, S. PRIMA, P. COUPÉ, S. MORRISSEY, AND C. BARILLOT, *Non-local means variants for denoising of diffusion-weighted and diffusion tensor mri*, in Medical Image Computing and Computer-Assisted Intervention–MICCAI 2007, Springer Berlin Heidelberg, 2007, pp. 344–351.

[38] ———, *Rician noise removal by non-local means filtering for low signal-to-noise ratio mri: Applications to dt-mri*, in Medical Image Computing and Computer-Assisted Intervention–MICCAI 2008, Springer Berlin Heidelberg, 2008, pp. 171–179.

[39] J. WOOD AND K. JOHNSON, *Wavelet packet denoising of magnetic resonance images: importance of rician noise at low snr*, Magnetic Resonance in Medicine, 41 (1999), pp. 631–635.

[40] C. WU AND X. TAI, *Augmented lagrangian method, dual methods, and split bregman iteration for rof, vectorial tv, and high order models*, SIAM J. Imaging Sci., 3 (2010), pp. 300–339.

[41] B. ZHANG, J. FADILI, AND J. STARCK, *Wavelets, ridgelets, and curvelets for poisson noise*

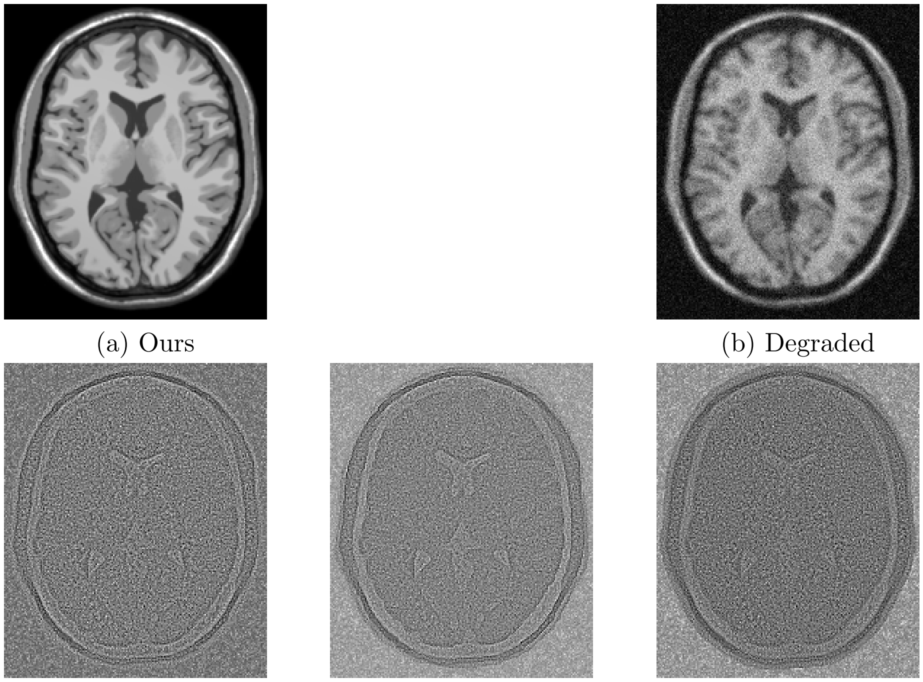

(a) Ours (b) Degraded

(c) ROF (d) Getreuer's (e) Ours

Fig. 6.7. *Residuals of different methods when restoring the degraded images corrupted by Gaussian blur and then Rician noise with $\sigma = 15$. Row 1: Original image and degraded image. Row 2 : recovered images with different methods. (a) Original "Brain", (b) degraded "Brain", (c) ROF model ($\lambda = 0.2$), (d) Getreuer's model ($\lambda = 50$;), (e) our method ($\gamma = 0.03$)*

removal, IEEE Trans Image Process., 17 (2008), pp. 1093–1108.

[42] M. Zhu, S. Wright, and T. Chan, *Duality-based algorithms for total-variation-regularized image restoration*, Comput. Optim. and Appl., 47 (2010), pp. 377–400.